On the compressible Hart-McClure and Sellars mean flow motions

Brian A. Maicke,[a] Tony Saad,[b] and Joseph Majdalani[c]
Department of Mechanical, Aerospace and Biomedical Engineering, University of Tennessee (UTSI), Tullahoma, Tennessee 37388-9700, USA

(Received 24 October 2011; accepted 3 August 2012; published online 6 September 2012)

We consider the compressible flow analogue of the solution known colloquially as the Hart-McClure profile. This potential motion is used to describe the mean flow in the original energy-based combustion instability framework. In this study, we employ the axisymmetric compressible form of the potential equation for steady, inviscid, irrotational flow assuming uniform injection of a calorically perfect gas in a porous, right-cylindrical chamber. This equation is expanded to order $\mathbf{M}_w^4$ using a Rayleigh-Janzen sequence in powers of $\mathbf{M}_w^2$, where $\mathbf{M}_w$ is the wall Mach number. At leading order, we readily recover the original Hart-McClure profile and, at $\mathbf{M}_w^2$, a closed-form representation of the compressible correction. By way of confirmation, the same solution is re-constructed using a novel application of the vorticity-streamfunction technique. In view of the favorable convergence properties of the Rayleigh-Janzen expansion, the resulting approximation can be relied upon from the headwall down to the sonic point and slightly beyond in a long porous tube or nozzleless chamber. As a windfall, the compressible Sellars motion that arises in the reverse flow problem driven by wall suction is deduced. Based on the simple closed-form expressions that prescribe this motion, the principal flow attributes are quantified parametrically and compared to existing incompressible and one-dimensional theories. In this effort, the local Mach number and pressure are calculated and shown to provide an improved formulation when gauged against one-dimensional theory. Our results are also compared to the two-dimensional axisymmetric solution obtained by Majdalani ["On steady rotational high speed flows: The compressible Taylor-Culick profile," Proc. R. Soc. London, Ser. A **463**, 131–162 (2007)]. After rescaling the axial coordinate by the critical length L_s, a parametrically-free form is obtained that is essentially independent of the Mach number. This behavior is verified analytically, thus confirming Majdalani's geometric similarity with respect to the critical distance. A secondary verification by computational fluid dynamics is also undertaken. When compared to existing rotational models, the compressible Hart-McClure plug-flow requires, as it should, a slightly longer distance to reach the speed of sound at the centerline. With this model, however, not only the centerline but the entire cross-section becomes fully choked. [http://dx.doi.org/10.1063/1.4748349]

I. INTRODUCTION

Despite the preponderance of potential solutions for describing various conceivable motions in external and internal aerodynamics, a review of the literature surprisingly reveals a dearth of analytical models that can be extended to high speed settings where compressibility emerges as a major contributor. Hill's 1894 spherical vortex[2] constitutes one such example that had to linger over

[a]Currently, Assistant Professor of Mechanical Engineering, The Pennsylvania State University, Middletown, PA 17057.
[b]Currently, Research Associate, Institute for Clean and Secure Energy, University of Utah, UT 84112.
[c]Author to whom correspondence should be addressed. Electronic mail: drmajdalani@gmail.com. Telephone: (931) 393-7280. Fax: (931) 393-7444. Web: http://majdalani.net.

a century before receiving attention in Moore and Pullin's compressible flow analysis in 1998.[3] In this vein, it may be safely argued that the scarcity of closed-form compressible models is not only germane to potential motions insofar as rotational problems share a similar disposition. The shortage of mathematical formulations associated with bounded fluids is even more substantial, as alluded to in recent articles on the subject.[1,4]

The development of a compressible rotational or irrotational solution is not only relevant in the context in which it appears, such as to better understand a mechanism or predict its general characteristics, but more importantly perhaps, it serves to provide the much needed benchmarks that are required to verify codes or test new theoretical concepts in the field, such as Kelvin's theorem for open regions,[5,6] and thereby help to advance the mathematical foundations of fluid mechanics in general, and compressible flow theory in particular. This can be seen in a study by Saad and Majdalani[6] who, in their effort at extending Kelvin's minimum energy theorem, surveyed the literature in search for multidimensional solutions that could be posed as testbeds for the treatment of ducted fluids with open boundaries. While incompressible solutions could be located with relative ease, the identification of compressible flow profiles with suitable characteristics proves far more entreating.

Along similar lines, Wasistho, Balachandar, and Moser[7] have argued that analytical representations can become an extraordinary resource for verifying numerical simulations in rocket motors. This is partly due to the challenges entailed in acquiring specific experimental measurements and, partly, as a consequence of the harsh environment arising in rocket chambers. In the same article, Wasistho *et al.*[7] suggest the use of a compressible mean flow profile in hydrodynamic instability calculations because of the heightened sensitivity displayed by their solutions on the base flow description. Their steady and unsteady results are subsequently compared to predictions derived from an integral formulation and, for the unsteady part, from a time-dependent expression for the oscillatory field by Majdalani and Van Moorhem.[8] Evidently, the favorable agreement and verification avenues reported by these researchers were contingent on the availability of reliable approximations.

This dichotomy in modeling approaches is only exacerbated with the advent of computer simulations. These are so heavily relied upon today that they have nearly superseded and fully displaced most of the formerly adopted methodologies. By way of example, the problem of simulating the internal mean flow in solid rocket motors has prompted several investigators within the propulsion community either to utilize Navier-Stokes solvers, such as Wasistho, Balachandar, and Moser,[7] Chedevergne, Casalis, and Majdalani,[9] Venugopal, Moser, and Najjar,[10] Beddini,[11] Sabnis, Gibeling and McDonald,[12] Liou and Lien,[13] or to pursue simplified integral formulations that can be evaluated numerically, such as Traineau, Hervat, and Kuentzmann,[14] Balakrishnan, Liñan, and Williams,[15,16] Akiki and Majdalani,[17] and others. But as far as the analytical modeling of the compressible base flow is concerned, a rather limited number of studies may be cited, and these comprise, besides the authors' efforts,[1,4] work by Gany and Aharon[18] along with a few others. The motivation for additional exploratory studies is clear. While reasons for this reduced emphasis may vary, they may be partly attributed to the mathematical challenges that arise in modeling compressible motions and the limited tools available to overcome the attendant complexities. In their compressible analysis of the porous channel flow, Maicke and Majdalani[4] provide an exposition of available numerical and analytical strategies, including those no longer in use, with special accent on the Rayleigh-Janzen expansion technique that will play a central role in this study.

Shifting attention to the steady-state velocity description in simulated rocket motors and porous tubes, several formulations have been systematically developed under incompressible, non-reactive chamber conditions. Examples include the irrotational model by McClure, Hart and Cantrell,[19] colloquially known as the Hart-McClure profile,[5] and the rotational equivalent by Taylor[20] and Culick,[21] often referred to as the Taylor-Culick mean flow. Following this tradition, other relevant models have been produced and these may be attributed to: Yuan and Finkelstein[22] who accounted for small viscosity, Majdalani and Saad[23] and Kurdyumov[24] who sought to accommodate arbitrary headwall injection and the effects of energy accumulation,[5] Sams *et al.*[25] and Kurdyumov[26] who incorporated the effects of wall taper and irregular cross-sections, and Majdalani *et al.*,[27,28] Zhou and Majdalani,[29] Xu *et al.*,[30] and Berbente, Dănăilă, and Berbente[31] who allowed for time-dependent

wall regression. Yet for those two-dimensional models in which compressibility is retained, a much shorter list may be identified. The ones we come across mainly consist of the compressible Taylor-Culick flow analogue in porous tubes,[1] and the equivalent solution in porous channels.[4]

Given the above-mentioned paradigm, it is the purpose of this study to pursue a compressible mean flow approximation corresponding to the Hart-McClure profile. Although simple in its inception, this model has played a key role in furthering the application of the energy balance method in a judiciously posed acoustic instability framework. Such a framework was carefully conceived by Hart, McClure, and co-workers in a number of classic investigations featuring, to name a few: Hart and McClure,[32,33] McClure, Hart, and Bird,[34] Cantrell, Hart, and McClure,[35] Hart and Cantrell,[36] McClure, Hart, and Cantrell,[19] Cantrell and Hart,[37] and Hart *et al.*[38] In fact, the energy-based methodology stands at the foundation of combustion instability analyses such as those undertaken by Flandro and Majdalani,[39] Fischbach, Majdalani and Flandro,[40] Majdalani, Flandro and Fischbach,[41] Majdalani, Fischbach, and Flandro,[42] and Flandro, Fischbach, and Majdalani.[43] One particular feature in the Hart-McClure injection pattern is the relaxation of the strictly radial velocity requirement at the sidewall. Such an assumption can prove helpful in the modeling of hybrid propellant rockets wherein a diffusion flame is established.[44,45] It will also facilitate the modeling of the thermal boundary layer in the presence of a simplified, albeit pseudo two-dimensional, mean flow expression.[46] From an academic standpoint, the linearized equations associated with this model can prove instrumental in leveraging the method of superposition while seeking to accommodate irregular boundary conditions.[47,48] Finally, given the growing emphasis on slip-boundary research in high speed applications, where slip boundaries facilitate the modeling of rarefied gases,[49,50] the quest for a compressible potential solution may be viewed as a worthy endeavor in its own right.

The paper is organized as follows. We begin by revisiting the Hart-McClure problem in an axisymmetric, constant diameter chamber with uniform and non-orthogonal wall injection. Then using a Rayleigh-Janzen series in even powers of the wall Mach number, we expand the compressible potential equation up to fourth order and extract the compressible flow analogue of Hart-McClure's. For added confirmation, the analysis is repeated using an equivalent approach based on the vorticity-streamfunction formulation. The compressible Sellars profile corresponding to the analogous but reverse flow problem driven by wall suction is also derived deductively. The compressible Hart-McClure approximation is then compared to one-dimensional theory, to its rotational counterpart, and to numerical simulations carried out under realistic turbulent conditions.

II. MATHEMATICAL MODEL

A. Geometry

We consider the steady, inviscid and non-heat conducting flow of an ideal gas in the domain bounded by the porous sidewall of a tube of radius a and finite length L_0. It is assumed that the non-orthogonal incoming speed of the gas at the wall has a radial component U_w and that L_0 can be sufficiently long to trigger sonic conditions. In solid and hybrid rockets, the sidewall velocity $U_w = \rho_P \dot{r}_P/\rho$ may be connected to the solid or fuel propellant regression rate, $\dot{r}_P$. To justify a constant U_w, we speculate that the streamwise depreciation in pressure and its wall-coupling effect can nearly offset the axial decrease in density. As shown in Fig. 1, $\bar{r}$ and $\bar{z}$ represent the radial and streamwise coordinates using a nomenclature in which the overbars denote dimensional quantities. All spatial variables are normalized by a in a coordinate system that has its origin at the headwall center. As usual, axial symmetry reduces the field investigation to the region $0 \le r \le 1$ and $0 \le z \le L$, where $L = L_0/a$ stands for the aspect ratio.

The tube can be taken to be closed at $z = 0$, corresponding to an inert headwall, and a sidewall velocity that conforms to the Hart-McClure profile, $\phi = -\frac{1}{2}r^2 + z^2$ (Fig. 1(a)). This configuration will be the main focus here with a slip-boundary at the sidewall. However, it is also possible to superimpose a headwall injection profile at $z = 0$ with characteristic speed U_c. The equivalent Taylor-Culick mean flow, $\psi = z\sin(\frac{1}{2}\pi r^2)$, is illustrated in Fig. 1(b) where the orthogonality of the injected fluid is showcased. The incompressible model of this problem was treated by Majdalani and Saad,[23] whereas the compressible flow analogue was analyzed by Majdalani.[1] The resulting

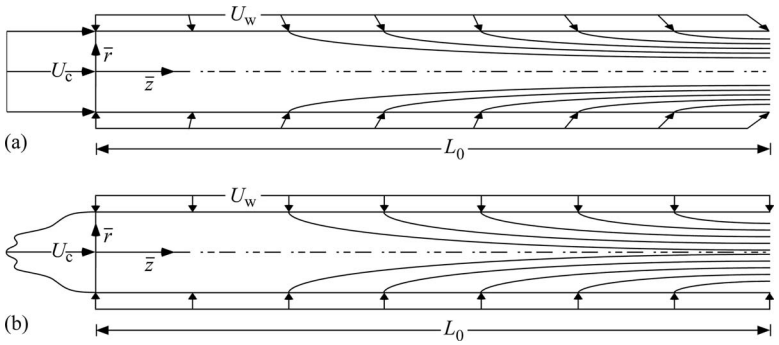

FIG. 1. Schematic of a porous tube with a transpiring sidewall along which flow can enter in accordance with (a) the Hart-McClure and (b) Taylor-Culick injection profiles. Headwall injection can be arbitrary but axisymmetric.

streamlines can be either induced by the injection process or by the two converging streams. The flowfield with headwall injection may be useful in modeling the bulk gaseous motion in hybrid rockets where U_w can be appreciably smaller than the average velocity of the oxidizer stream, U_c. Typical hybrids exhibit values of $U_c/U_w \sim O(10^2 - 10^3)$ and $M_w = U_w/c_0 \sim O(10^{-4})$, where c_0 is the speed of sound. In seeking an exact potential solution in the Hart-McClure case, it is necessary for the headwall injection velocity to be irrotational and, therefore, invariant in the radial direction (i.e., uniform). Otherwise, only an approximate result may be obtained, as shown by Majdalani and Saad[23] in their rotational analysis of this problem with arbitrary headwall injection. In what follows, the steps leading to a compressible potential approximation will be delineated, although the addition of a secondary stream at the headwall can be achieved by way of superposition.

B. Nomenclature and boundary conditions

We begin by normalizing the fundamental flow variables and operators using standard axisymmetric descriptors. These can be written as

$$u_r = \frac{\bar{u}_r}{U_w}, \quad u_z = \frac{\bar{u}_z}{U_w}, \quad p = \frac{\bar{p}}{p_0}, \quad T = \frac{\bar{T}}{T_0}, \quad \rho = \frac{\bar{\rho}}{\rho_0}, \quad \phi = \frac{\bar{\phi}}{aU_w}, \quad \psi = \frac{\bar{\psi}}{a^2\rho U_w}, \quad \mathbf{\Omega} = \frac{\bar{\mathbf{\Omega}}a}{U_w},$$
$$\nabla = a\bar{\nabla}, \quad \nabla^2 = a^2\bar{\nabla}^2, \tag{1}$$

where ϕ, ψ, and $\mathbf{\Omega}$ denote the potential function, streamfunction, and vorticity, respectively. The latter may be referenced in connection with the Taylor-Culick model. The subscript '0' refers to conditions at the origin; $U_c = \bar{u}_z(0, 0)$ and $U_w = -\bar{u}_r(a, \bar{z})$ define the injection constants along the headwall and sidewall, respectively. As usual, the velocity, Stokes streamfunction, and potential function are related through

$$\mathbf{u} = u_r\mathbf{e}_r + u_z\mathbf{e}_z = \frac{\partial\phi}{\partial r}\mathbf{e}_r + \frac{\partial\phi}{\partial z}\mathbf{e}_z = -\frac{1}{\rho r}\frac{\partial\psi}{\partial z}\mathbf{e}_r + \frac{1}{\rho r}\frac{\partial\psi}{\partial r}\mathbf{e}_z. \tag{2}$$

Given an isentropic flow of a calorically perfect gas with $\gamma \equiv c_p/c_v$, one can also take

$$\rho = p^{1/\gamma} \text{ and } T = p^{1-1/\gamma}. \tag{3}$$

Our auxiliary conditions are prescribed by the continuity of the flow across the centerline and radial inflow conditions at the sidewall that are consistent with both the Hart-McClure and Taylor-Culick representations. Headwall injection can be imposed on the streamwise component in the event of an open boundary. In adhering to the original Hart-McClure model, we begin by considering the

case of no flow at $z = 0$. This assortment of conditions can be expressed by

$$\begin{cases} \bar{r}=0,\ \forall \bar{z},\ \bar{u}_r=0 & \text{(no flow across centerline)} \\ \bar{r}=0,\ \bar{z}=0,\ \bar{\phi}=0 & \text{(datum for potential flow)} \\ \bar{r}=a, 0 \le \bar{z} < L_0,\ \bar{u}_r=-U_{\mathrm{w}} & \text{(uniform sidewall injection)} \\ \bar{z}=0,\ \forall \bar{r},\ \bar{u}_z=0 & \text{(no headwall injection)} \end{cases} \text{ and so } \begin{cases} u_r(0,z)=\dfrac{\partial \phi(0,z)}{\partial r}=0 \\ \phi(0,0)=0 \\ u_r(1,z)=\dfrac{\partial \phi(1,z)}{\partial r}=-1 \\ u_z(r,0)=\dfrac{\partial \phi(r,0)}{\partial z}=0 \end{cases}. \tag{4}$$

At this juncture, a solution that satisfies Eq. (4) may be derived from the compressible form of the potential equation and then substituted back into the momentum equation so that the pressure is deduced. Isentropic relations can then be employed to calculate the density and temperature.

C. Potential flow equation

To derive the potential flow equation we begin with the continuity equation written in dimensional variables,

$$\frac{\partial}{\partial \bar{r}}(\bar{\rho}\bar{u}_r\bar{r}) + \frac{\partial}{\partial \bar{\theta}}(\bar{\rho}\bar{u}_\theta) + \bar{r}\frac{\partial}{\partial \bar{z}}(\bar{\rho}\bar{u}_z) = 0. \tag{5}$$

To simplify matters, the tangential derivative is eliminated assuming axisymmetric motion. The result is an expanded version of Eq. (5) with

$$\bar{r}\left[\bar{u}_r\frac{\partial \bar{\rho}}{\partial \bar{r}} + \bar{u}_z\frac{\partial \bar{\rho}}{\partial \bar{z}} + \bar{\rho}\left(\frac{\partial \bar{u}_r}{\partial \bar{r}} + \frac{\partial \bar{u}_z}{\partial \bar{z}}\right)\right] + \bar{\rho}\bar{u}_r = 0. \tag{6}$$

The potential function is then introduced via

$$\bar{u}_r = \frac{\partial \bar{\phi}}{\partial \bar{r}} \text{ and } \bar{u}_z = \frac{\partial \bar{\phi}}{\partial \bar{z}}. \tag{7}$$

Substituting Eq. (7) into Eq. (6) yields

$$\bar{\rho}\left(\frac{\partial^2 \bar{\phi}}{\partial \bar{r}^2} + \frac{1}{\bar{r}}\frac{\partial \bar{\phi}}{\partial \bar{r}} + \frac{\partial^2 \bar{\phi}}{\partial \bar{z}^2}\right) = -\frac{\partial \bar{\phi}}{\partial \bar{r}}\frac{\partial \bar{\rho}}{\partial \bar{r}} - \frac{\partial \bar{\phi}}{\partial \bar{z}}\frac{\partial \bar{\rho}}{\partial \bar{z}}. \tag{8}$$

The density terms must be eliminated to reach the desired potential equation. We recall that

$$\mathrm{d}\bar{p} = -\frac{\bar{\rho}}{2}\mathrm{d}\left[\left(\frac{\partial \bar{\phi}}{\partial \bar{r}}\right)^2 + \left(\frac{\partial \bar{\phi}}{\partial \bar{z}}\right)^2\right], \tag{9}$$

where the "d" operator represents an exact derivative. Equation (9) represents Euler's equation in axisymmetric cylindrical coordinates. Realizing that the flow is isentropic, it is possible to express the speed of sound as

$$c^2 = \frac{\mathrm{d}\bar{p}}{\mathrm{d}\bar{\rho}} \quad \text{or} \quad \mathrm{d}\bar{\rho} = \frac{\mathrm{d}\bar{p}}{c^2}. \tag{10}$$

Here c is the local speed of sound and not a reference value. Equation (10) provides the means to eliminate the density from Eq. (8). This can be seen by combining Eqs. (9) and (10) into

$$\mathrm{d}\bar{\rho} = -\frac{\bar{\rho}}{2c^2}\mathrm{d}\left[\left(\frac{\partial \bar{\phi}}{\partial \bar{r}}\right)^2 + \left(\frac{\partial \bar{\phi}}{\partial \bar{z}}\right)^2\right] \tag{11}$$

or

$$\begin{aligned}\frac{\partial \bar{\rho}}{\partial \bar{r}}\mathrm{d}\bar{r} + \frac{\partial \bar{\rho}}{\partial \bar{z}}\mathrm{d}\bar{z} = -\frac{\bar{\rho}}{2c^2}\Bigg[&2\frac{\partial \bar{\phi}}{\partial \bar{r}}\frac{\partial}{\partial \bar{r}}\left(\frac{\partial \bar{\phi}}{\partial \bar{r}}\right)\mathrm{d}\bar{r} + 2\frac{\partial \bar{\phi}}{\partial \bar{r}}\frac{\partial}{\partial \bar{z}}\left(\frac{\partial \bar{\phi}}{\partial \bar{r}}\right)\mathrm{d}\bar{z} + 2\frac{\partial \bar{\phi}}{\partial \bar{z}}\frac{\partial}{\partial \bar{r}}\left(\frac{\partial \bar{\phi}}{\partial \bar{z}}\right)\mathrm{d}\bar{r} \\ &+2\frac{\partial \bar{\phi}}{\partial \bar{z}}\frac{\partial}{\partial \bar{z}}\left(\frac{\partial \bar{\phi}}{\partial \bar{z}}\right)\mathrm{d}\bar{z}\Bigg].\end{aligned} \tag{12}$$

Collecting partial differentials in $\mathrm{d}\bar{r}$ and $\mathrm{d}\bar{z}$ and simplifying, we get

$$\begin{cases} \dfrac{\partial \bar{\rho}}{\partial \bar{r}} = -\dfrac{\bar{\rho}}{c^2}\left(\dfrac{\partial \bar{\phi}}{\partial \bar{r}}\dfrac{\partial^2 \bar{\phi}}{\partial \bar{r}^2} + \dfrac{\partial \bar{\phi}}{\partial \bar{z}}\dfrac{\partial^2 \bar{\phi}}{\partial \bar{r}\partial \bar{z}}\right) \\ \dfrac{\partial \bar{\rho}}{\partial \bar{z}} = -\dfrac{\rho}{c^2}\left(\dfrac{\partial \bar{\phi}}{\partial \bar{z}}\dfrac{\partial^2 \bar{\phi}}{\partial \bar{z}^2} + \dfrac{\partial \bar{\phi}}{\partial \bar{r}}\dfrac{\partial^2 \bar{\phi}}{\partial \bar{r}\partial \bar{z}}\right) \end{cases}. \tag{13}$$

At this point, inserting Eq. (13) into Eq. (8) suppresses the density differentials and produces

$$\bar{\nabla}^2\bar{\phi} = \frac{1}{c^2}\left[\left(\frac{\partial \bar{\phi}}{\partial \bar{r}}\right)^2\frac{\partial^2 \bar{\phi}}{\partial \bar{r}^2} + \left(\frac{\partial \bar{\phi}}{\partial \bar{z}}\right)^2\frac{\partial^2 \bar{\phi}}{\partial \bar{z}^2} + 2\frac{\partial \bar{\phi}}{\partial \bar{r}}\frac{\partial \bar{\phi}}{\partial \bar{z}}\frac{\partial^2 \bar{\phi}}{\partial \bar{r}\partial \bar{z}}\right]. \tag{14}$$

Because c remains a local speed of sound, it must be expanded to account for the implied velocity potentials that it contains. When expressed in terms of its stagnation value, we get

$$c^2 = c_0^2 - \frac{\gamma - 1}{2}\left[\left(\frac{\partial \bar{\phi}}{\partial \bar{r}}\right)^2 + \left(\frac{\partial \bar{\phi}}{\partial \bar{z}}\right)^2\right], \tag{15}$$

where c_0 is the speed of sound at stagnation conditions, often taken at the inert headwall. Equation (14) becomes

$$\left\{1 - \frac{\gamma - 1}{2c_0^2}\left[\left(\frac{\partial \bar{\phi}}{\partial \bar{r}}\right)^2 + \left(\frac{\partial \bar{\phi}}{\partial \bar{z}}\right)^2\right]\right\}\bar{\nabla}^2\bar{\phi} = \frac{1}{c_0^2}\left[\left(\frac{\partial \bar{\phi}}{\partial \bar{r}}\right)^2\frac{\partial^2 \bar{\phi}}{\partial \bar{r}^2} + \left(\frac{\partial \bar{\phi}}{\partial \bar{z}}\right)^2\frac{\partial^2 \bar{\phi}}{\partial \bar{z}^2} + 2\frac{\partial \bar{\phi}}{\partial \bar{r}}\frac{\partial \bar{\phi}}{\partial \bar{z}}\frac{\partial^2 \bar{\phi}}{\partial \bar{r}\partial \bar{z}}\right]. \tag{16}$$

Applying the normalization designated in Eq. (1) adds a U_{w}^2 term to the elements that are divided by c_0^2. This leaves us with the compressible, two-dimensional, axisymmetric form of the potential equation, specifically

$$\begin{aligned} &\left\{1 - M_{\mathrm{w}}^2\frac{\gamma - 1}{2}\left[\left(\frac{\partial \phi}{\partial r}\right)^2 + \left(\frac{\partial \phi}{\partial z}\right)^2\right]\right\}\nabla^2\phi \\ &\quad = M_{\mathrm{w}}^2\left[\left(\frac{\partial \phi}{\partial r}\right)^2\frac{\partial^2 \phi}{\partial r^2} + \left(\frac{\partial \phi}{\partial z}\right)^2\frac{\partial^2 \phi}{\partial z^2} + 2\frac{\partial \phi}{\partial r}\frac{\partial \phi}{\partial z}\frac{\partial^2 \phi}{\partial r\partial z}\right]. \end{aligned} \tag{17}$$

III. SOLUTION

A. Rayleigh-Janzen expansion

The compressible potential flow equation[51] is subject to four boundary conditions associated with the Taylor-Culick irrotational flow, known colloquially as the Hart-McClure profile. These conditions correspond to: (a) an impermeable headwall, (b) no radial flow across the centerline, (c) a radial sidewall velocity equal to the injection velocity, and (d) a vanishing reference potential at the center of the headwall. Mathematically, these requirements translate into

$$\frac{\partial \phi}{\partial z}(r, 0) = 0, \quad \frac{\partial \phi}{\partial r}(0, z) = 0, \quad \frac{\partial \phi}{\partial r}(1, z) = -1, \quad \phi(0, 0) = 0. \tag{18}$$

In retrospect, the above conditions are similar to those used by Culick[21] except for the no-slip requirement which is not needed here. Equation (17) may be rearranged into

$$\nabla^2\phi = M_{\mathrm{w}}^2\left\{\left(\frac{\partial \phi}{\partial r}\right)^2\frac{\partial^2 \phi}{\partial r^2} + \left(\frac{\partial \phi}{\partial z}\right)^2\frac{\partial^2 \phi}{\partial z^2} + 2\frac{\partial \phi}{\partial r}\frac{\partial \phi}{\partial z}\frac{\partial^2 \phi}{\partial r\partial z} + \frac{\gamma - 1}{2}\left[\left(\frac{\partial \phi}{\partial r}\right)^2 + \left(\frac{\partial \phi}{\partial z}\right)^2\right]\nabla^2\phi\right\}. \tag{19}$$

At this stage, a Rayleigh-Janzen expansion in the square of the Mach number may be called upon. This expansion is based on

$$\phi(r,z) = \phi_0(r,z) + M_{\mathrm{w}}^2\phi_1(r,z) + O(M_{\mathrm{w}}^4). \tag{20}$$

Substituting Eq. (20) into Eq. (19) yields, after some cancellations,

$$\begin{aligned}
&\left(\frac{\partial^2\phi_0}{\partial r^2} + \frac{1}{r}\frac{\partial\phi_0}{\partial r} + \frac{\partial^2\phi_0}{\partial z^2}\right) + M_{\mathrm{w}}^2\left(\frac{\partial^2\phi_1}{\partial r^2} + \frac{1}{r}\frac{\partial\phi_1}{\partial r} + \frac{\partial^2\phi_1}{\partial z^2}\right)\\
&= M_{\mathrm{w}}^2\left\{\left(\frac{\partial\phi_0}{\partial r}\right)^2\frac{\partial^2\phi_0}{\partial r^2} + \left(\frac{\partial\phi_0}{\partial z}\right)^2\frac{\partial^2\phi_0}{\partial z^2} + 2\frac{\partial\phi_0}{\partial r}\frac{\partial\phi_0}{\partial z}\frac{\partial^2\phi_0}{\partial r\partial z}\right.\\
&\quad\left. + \frac{\gamma-1}{2}\left[\left(\frac{\partial\phi_0}{\partial r}\right)^2 + \left(\frac{\partial\phi_0}{\partial z}\right)^2\right]\nabla^2\phi_0\right\} + O(M_w^4).
\end{aligned} \tag{21}$$

Similarly, to determine the thermodynamic variables, we can expand Eq. (9) using

$$\begin{cases} p(r,z) = 1 + M_{\mathrm{w}}^2 p_1(r,z) + M_{\mathrm{w}}^4 p_2(r,z) + O(M_{\mathrm{w}}^6) \\ \rho(r,z) = 1 + M_{\mathrm{w}}^2\rho_1(r,z) + M_{\mathrm{w}}^4\rho_2(r,z) + O(M_{\mathrm{w}}^6) \end{cases}. \tag{22}$$

Finally, the substitution of Eq. (22) into Eq. (9) engenders

$$\begin{aligned}
\mathrm{d}\left(1 + M_{\mathrm{w}}^2 p_1 + M_{\mathrm{w}}^4 p_2\right) = -\gamma M_{\mathrm{w}}^2\left(\frac{1 + M_{\mathrm{w}}^2\rho_1 + M_{\mathrm{w}}^4\rho_2}{2}\right)\mathrm{d}\left\{\left[\frac{\partial\left(\phi_0 + M_{\mathrm{w}}^2\phi_1\right)}{\partial r}\right]^2\right.\\
\left. + \left[\frac{\partial\left(\phi_0 + M_{\mathrm{w}}^2\phi_1\right)}{\partial z}\right]^2\right\}.
\end{aligned} \tag{23}$$

Here the γM_{w}^2 term emerges as a byproduct of the normalization in Eq. (9) and the relation $p_0/\rho_0 = c_0^2/\gamma$. The latter will be expanded as needed to deduce the pressure at successive orders.

B. Leading-order solution

At $O(1)$, one identifies

$$\frac{\partial^2\phi_0}{\partial r^2} + \frac{1}{r}\frac{\partial\phi_0}{\partial r} + \frac{\partial^2\phi_0}{\partial z^2} = 0. \tag{24}$$

Then using $\phi_0(r,z) = f_0(r) + g_0(z)$, one obtains

$$\frac{\mathrm{d}^2 f_0}{\mathrm{d}r^2} + \frac{1}{r}\frac{\mathrm{d}f_0}{\mathrm{d}r} + \frac{\mathrm{d}^2 g_0}{\mathrm{d}z^2} = 0 \quad \text{or} \quad \frac{\mathrm{d}^2 f_0}{\mathrm{d}r^2} + \frac{1}{r}\frac{\mathrm{d}f_0}{\mathrm{d}r} = -\frac{\mathrm{d}^2 g_0}{\mathrm{d}z^2} \equiv \upsilon, \tag{25}$$

where υ represents the separation constant. At this juncture, the assortment of physical requirements seems to dictate the separation scheme to be pursued. In our case, the use of additive separation of variables enables us to satisfy all of the boundary conditions. In contrast, the use of multiplicative separation prevents us from securing the radial boundary condition at the centerline. In other problems, the converse may be true. To proceed, integration in the two space coordinates may be carried out straightforwardly. One gets

$$\begin{cases} \dfrac{\mathrm{d}^2 f_0}{\mathrm{d}r^2} + \dfrac{1}{r}\dfrac{\mathrm{d}f_0}{\mathrm{d}r} = \upsilon, \quad f_0(r) = \frac{1}{4}\upsilon r^2 + C_1\ln r + C_2 \\ -\dfrac{\mathrm{d}^2 g_0}{\mathrm{d}z^2} = \upsilon, \quad g_0(z) = -\frac{1}{2}\upsilon z^2 + C_3 z + C_4 \end{cases}. \tag{26}$$

The boundary conditions can now be used to extract

$$\frac{\partial \phi_0(r,0)}{\partial z} = 0, \quad \frac{\mathrm{d}g_0(0)}{\mathrm{d}z} = 0 \rightarrow \quad C_3 = 0, \tag{27}$$

$$\frac{\partial \phi_0(0,z)}{\partial r} = 0, \quad \frac{\mathrm{d}f_0(0)}{\mathrm{d}r} = 0 \rightarrow \quad C_1 = 0, \tag{28}$$

$$\frac{\partial \phi_0(1,z)}{\partial r} = -1, \quad \frac{\mathrm{d}f_0(1)}{\mathrm{d}r} = -1 \rightarrow \quad \upsilon = -2, \tag{29}$$

$$\phi_0(0,0) = 0, \quad f_0(0) + g_0(0) = 0 \rightarrow \quad C_2 + C_4 = 0. \tag{30}$$

In total, we collect

$$f_0 = -\tfrac{1}{2}r^2 + C_2, \quad g_0 = z^2 + C_4 \tag{31}$$

and so

$$\phi_0 = f_0 + g_0 = -\tfrac{1}{2}r^2 + z^2 + C_2 + C_4. \tag{32}$$

Because C_2 and C_4 are strictly additive constants that do not multiply any other term, they can both be set equal to zero without loss of generality. Then by virtue of Eq. (30), we are left with

$$\phi_0 = -\tfrac{1}{2}r^2 + z^2. \tag{33}$$

We thus recover the irrotational, incompressible, inviscid solution, which is often referred to in the propulsion community as the Hart-McClure profile.[32,35,37] This profile was the precursor to Culick's model and constitutes one of the first base flows used to study combustion instability in solid rocket motors. Outside the realm of propulsion, the same solution is used to model flow around a cavity. Its velocity components are simply given by

$$u_r = -r, \quad u_\theta = 0, \quad u_z = 2z. \tag{34}$$

So while it satisfies mass conservation, it remains irrotational. The leading-order pressure may be easily obtained from retaining the $O(M_\mathrm{w}^2)$ elements of Eq. (23), namely

$$\mathrm{d}p_1 = -\tfrac{1}{2}\gamma\,\mathrm{d}\left[\left(\frac{\partial \phi_0}{\partial r}\right)^2 + \left(\frac{\partial \phi_0}{\partial z}\right)^2\right]. \tag{35}$$

Integration of Eq. (35) generates

$$p_1 = -\tfrac{1}{2}\gamma\left(r^2 + 4z^2\right) \quad \text{and so} \quad p(r,z) = 1 - \tfrac{1}{2}\gamma\left(r^2 + 4z^2\right)M_\mathrm{w}^2 + O(M_\mathrm{w}^4). \tag{36}$$

Note that the constant of integration vanishes in view of the reference condition at the headwall.

C. First-order Mach number correction

At $O(M_\mathrm{w}^2)$, we retrieve from Eq. (21),

$$\nabla^2\phi_1 = \left(\frac{\partial \phi_0}{\partial r}\right)^2 \frac{\partial^2 \phi_0}{\partial r^2} + \left(\frac{\partial \phi_0}{\partial z}\right)^2 \frac{\partial^2 \phi_0}{\partial z^2} + 2\frac{\partial \phi_0}{\partial r}\frac{\partial \phi_0}{\partial z}\frac{\partial^2 \phi_0}{\partial r \partial z} + \frac{\gamma - 1}{2}\left[\left(\frac{\partial \phi_0}{\partial r}\right)^2 + \left(\frac{\partial \phi_0}{\partial z}\right)^2\right]\nabla^2\phi_0. \tag{37}$$

Equation (37) appears, at first glance, to be nearly intractable. However, it may be verified that the substitution of $\phi_0 = -\frac{1}{2}r^2 + z^2$ will prompt several simplifications that leave us simply with

$$\frac{\partial^2 \phi_1}{\partial r^2} + \frac{1}{r}\frac{\partial \phi_1}{\partial r} + \frac{\partial^2 \phi_1}{\partial z^2} = -r^2 + 8z^2. \tag{38}$$

As before, we posit a separable solution of the type $\phi_1(r,z)=f_1(r)+g_1(z)$. The same process is then repeated, starting with

$$\frac{\mathrm{d}^2 f_1}{\mathrm{d}r^2}+\frac{1}{r}\frac{\mathrm{d}f_1}{\mathrm{d}r}+\frac{\mathrm{d}^2 g_1}{\mathrm{d}z^2}=-r^2+8z^2. \tag{39}$$

The radial and axial functions may be readily segregated by putting

$$\frac{\mathrm{d}^2 f_1}{\mathrm{d}r^2}+\frac{1}{r}\frac{\mathrm{d}f_1}{\mathrm{d}r}+r^2=-\frac{\mathrm{d}^2 g_1}{\mathrm{d}z^2}+8z^2\equiv\kappa, \tag{40}$$

where κ denotes the separation constant. On the one hand, the radial function becomes

$$\frac{\mathrm{d}^2 f_1}{\mathrm{d}r^2}+\frac{1}{r}\frac{\mathrm{d}f_1}{\mathrm{d}r}+r^2=\kappa,\quad f_1(r)=\kappa\frac{r^2}{4}-\frac{r^4}{16}+K_1\ln r+K_2. \tag{41}$$

On the other hand, we collect in the axial direction,

$$-\frac{\mathrm{d}^2 g_1}{\mathrm{d}z^2}+8z^2=\kappa,\quad g_1(z)=\frac{2}{3}z^4-\frac{\kappa}{2}z^2+K_3z+K_4. \tag{42}$$

At this juncture, the boundary conditions may be applied to give

$$\begin{cases}\dfrac{\partial\phi_1(r,0)}{\partial z}=0, & \dfrac{\mathrm{d}g_1(0)}{\mathrm{d}z}=0\rightarrow \quad K_3=0\\[2ex] \dfrac{\partial\phi_1(0,z)}{\partial r}=0, & \dfrac{\mathrm{d}f_1(0)}{\mathrm{d}r}=0\rightarrow \quad K_1=0\\[2ex] \dfrac{\partial\phi_1(1,z)}{\partial r}=0, & \dfrac{\mathrm{d}f_1(1)}{\mathrm{d}r}=0\rightarrow \quad \kappa=\dfrac{1}{2}\\[2ex] \phi_1(0,0)=0, & f_1(0)+g_1(0)=0\rightarrow \quad K_2+K_4=0\end{cases}. \tag{43}$$

Backward substitution of Eq. (43) leads to

$$\phi_1(r,z)=\tfrac{1}{8}r^2-\tfrac{1}{16}r^4+\tfrac{2}{3}z^4-\tfrac{1}{4}z^2. \tag{44}$$

At length, combining leading and first-order contributions, we arrive at

$$\phi(r,z)=\phi_0+M_{\mathrm{w}}^2\phi_1+O(M_{\mathrm{w}}^4)=-\tfrac{1}{2}r^2+z^2+(\tfrac{1}{8}r^2-\tfrac{1}{16}r^4+\tfrac{2}{3}z^4-\tfrac{1}{4}z^2)M_{\mathrm{w}}^2+O(M_{\mathrm{w}}^4) \tag{45}$$

and so, finally,

$$\phi(r,z)=-\tfrac{1}{2}r^2+z^2+\tfrac{1}{48}\left[3(2-r^2)r^2+4(8z^2-3)z^2\right]M_{\mathrm{w}}^2+O(M_{\mathrm{w}}^4). \tag{46}$$

With the advent of Eq. (46), the velocity and pressure fields may be readily derived, namely,

$$\begin{cases}u_r=-r+\tfrac{1}{4}(1-r^2)rM_{\mathrm{w}}^2+O(M_{\mathrm{w}}^4)\\ u_z=2z+\tfrac{1}{6}(16z^2-3)zM_{\mathrm{w}}^2+O(M_{\mathrm{w}}^4)\end{cases}. \tag{47}$$

To circumvent the introduction of the density in the $O(M_{\mathrm{w}}^4)$ Euler equation, we segregate the total differentials into their partial components by putting

$$\begin{cases}\dfrac{\partial p_2}{\partial r}=-\gamma\left[\rho_1\left(\dfrac{\partial\phi_0}{\partial r}\dfrac{\partial^2\phi_0}{\partial r^2}+\dfrac{\partial\phi_0}{\partial z}\dfrac{\partial^2\phi_0}{\partial r\partial z}\right)+\dfrac{\partial\phi_0}{\partial r}\dfrac{\partial^2\phi_1}{\partial r^2}+\dfrac{\partial\phi_1}{\partial r}\dfrac{\partial^2\phi_0}{\partial r^2}+\dfrac{\partial\phi_1}{\partial z}\dfrac{\partial^2\phi_0}{\partial r\partial z}+\dfrac{\partial\phi_0}{\partial z}\dfrac{\partial^2\phi_1}{\partial r\partial z}\right]\\[2ex] \dfrac{\partial p_2}{\partial z}=-\gamma\left[\rho_1\left(\dfrac{\partial\phi_0}{\partial z}\dfrac{\partial^2\phi_0}{\partial z^2}+\dfrac{\partial\phi_0}{\partial r}\dfrac{\partial^2\phi_0}{\partial r\partial z}\right)+\dfrac{\partial\phi_0}{\partial z}\dfrac{\partial^2\phi_1}{\partial z^2}+\dfrac{\partial\phi_1}{\partial z}\dfrac{\partial^2\phi_0}{\partial z^2}+\dfrac{\partial\phi_1}{\partial r}\dfrac{\partial^2\phi_0}{\partial r\partial z}+\dfrac{\partial\phi_0}{\partial r}\dfrac{\partial^2\phi_1}{\partial r\partial z}\right]\end{cases}. \tag{48}$$

The nature of the potential solution precludes the existence of mixed differential terms, thus simplifying Eq. (48) to

$$\begin{cases} \dfrac{\partial p_2}{\partial r} = -\gamma \left[\rho_1 \left(\dfrac{\partial \phi_0}{\partial r} \dfrac{\partial^2 \phi_0}{\partial r^2} \right) + \dfrac{\partial \phi_0}{\partial r} \dfrac{\partial^2 \phi_1}{\partial r^2} + \dfrac{\partial \phi_1}{\partial r} \dfrac{\partial^2 \phi_0}{\partial r^2} \right] \\ \dfrac{\partial p_2}{\partial z} = -\gamma \left[\rho_1 \left(\dfrac{\partial \phi_0}{\partial z} \dfrac{\partial^2 \phi_0}{\partial z^2} \right) + \dfrac{\partial \phi_0}{\partial z} \dfrac{\partial^2 \phi_1}{\partial z^2} + \dfrac{\partial \phi_1}{\partial z} \dfrac{\partial^2 \phi_0}{\partial z^2} \right] \end{cases}. \tag{49}$$

As the right-hand sides of both equations are known, integration of Eq. (49) with respect to r and z produces

$$\begin{cases} p_2 = -\gamma \left[\frac{1}{8} \left(r^4 - 2r^2 \right) - r^2 z^2 \right] + G(z) \\ p_2 = -\gamma \left[\frac{10}{3} z^4 - z^2 - r^2 z^2 \right] + F(r) \end{cases}. \tag{50}$$

The total pressure correction may be arrived at by combining the two members of Eq. (50); this can be accomplished while ensuring that common terms are not duplicated. Being an exact differential at each order, we get

$$p_2 = -\gamma \left[\tfrac{1}{8} \left(r^4 - 2r^2 \right) - r^2 z^2 + \tfrac{10}{3} z^4 - z^2 \right], \tag{51}$$

and so, by way of Eq. (22), we arrive at

$$p(r, z) = 1 - \tfrac{1}{2} \gamma \left(r^2 + 4z^2 \right) M_{\mathrm{w}}^2 - \gamma \left[\tfrac{1}{8} \left(r^4 - 2r^2 \right) - r^2 z^2 + \tfrac{10}{3} z^4 - z^2 \right] M_{\mathrm{w}}^4 + O(M_{\mathrm{w}}^6). \tag{52}$$

IV. VORTICITY-STREAMFUNCTION FORMULATION

An alternate approach may be pursued to derive and verify the results obtained heretofore. The corresponding analysis follows the so-called vorticity-streamfunction technique that is often employed in lieu of the potential function formulation, especially that the latter is limited to irrotational motions. The equivalent procedure may be initiated by expressing the statement of irrotationality in terms of the vorticity, namely,

$$\boldsymbol{\Omega} = \nabla \times \mathbf{u} = \mathbf{0}. \tag{53}$$

Then given $u_\theta = 0$, $u_r \neq u_r(\theta)$, and $u_z \neq u_z(\theta)$, the only relevant (i.e., not self-cancelling) component of vorticity is retained in the tangential direction, where the dimensionless form of Eq. (53) may be expanded into

$$\Omega_\theta = \frac{\partial u_r}{\partial z} - \frac{\partial u_z}{\partial r} = 0. \tag{54}$$

To eliminate the velocities, one may use a modified form of the Stokes streamfunction for compressible flows. Granted axisymmetric cylindrical coordinates, one can put, as per Eq. (2),

$$u_r = -\frac{1}{\rho r} \frac{\partial \psi}{\partial z} \quad \text{and} \quad u_z = \frac{1}{\rho r} \frac{\partial \psi}{\partial r}. \tag{55}$$

These relations may be readily substituted into Eq. (54) to retrieve the specific PDE for this problem,

$$\frac{\partial^2 \psi}{\partial r^2} - \frac{1}{r} \frac{\partial \psi}{\partial r} + \frac{\partial^2 \psi}{\partial z^2} = \frac{1}{\rho} \frac{\partial \rho}{\partial r} \frac{\partial \psi}{\partial r} + \frac{1}{\rho} \frac{\partial \rho}{\partial z} \frac{\partial \psi}{\partial z}. \tag{56}$$

Upon further inspection, it may be seen that Eq. (56) requires the determination of the density and, consequently, of the pressure field. In a Rayleigh-Janzen treatment of the form $\psi(r, z) = \psi_0 + M_{\mathrm{w}}^2 \psi_1 + O(M_{\mathrm{w}}^4)$, it may be shown that the solution lends itself to a strategy in which the Euler equations may be used to solve for the pressure, while the density may be recovered directly from the isentropic relation given by Eq. (3). In fact, a standard expansion in the square of the wall injection Mach number leads to the following leading and first-order solutions.

A. Leading-order solution

Using the same nomenclature as before, the leading-order set that we identify consists of

$$O(1): \quad \begin{cases} \nabla p_0 = 0 & \text{(Euler's equation)} \\ \rho_0 = p_0^{1/\gamma} = 1 & \text{(isentropic relation)} \\ \dfrac{\partial^2 \psi_0}{\partial r^2} - \dfrac{1}{r}\dfrac{\partial \psi_0}{\partial r} + \dfrac{\partial^2 \psi_0}{\partial z^2} = 0 & \text{(vorticity equation)} \end{cases}. \tag{57}$$

The boundary conditions associated with Eq. (57) must be consistent with those expressed by Eq. (18), with the streamfunction being set (arbitrarily) to vanish at the chamber headwall. We therefore have

$$\psi_0(0,0) = 0, \; u_r^{(0)}(0,z) = \lim_{r\to 0} \frac{1}{r}\frac{\partial \psi_0(r,z)}{\partial z} = 0, \; u_r^{(0)}(1,z) = \frac{1}{r}\frac{\partial \psi_0(1,z)}{\partial z} = 1,$$
$$u_z^{(0)}(r,0) = \frac{1}{r}\frac{\partial \psi_0(r,0)}{\partial r} = 0. \tag{58}$$

The ensuing ψ_0 may be straightforwardly obtained using separation of variables that are based on multiplicative functions of r and z. We get

$$\psi_0 = r^2 z, \quad u_r^{(0)} = -r, \quad u_z^{(0)} = 2z. \tag{59}$$

Equation (59) corresponds to the incompressible, irrotational form used by McClure, Hart and Cantrell[19] that preceded the advent of the Taylor-Culick model. It is discussed at length in a companion paper by Saad and Majdalani.[6]

B. First-order correction

The equations for the first-order system may be similarly deduced from the momentum, isentropic, and vorticity equations where all dependent variables are expanded in their respective Rayleigh-Janzen series. We collect

$$O(M_w^2): \quad \begin{cases} \nabla p_1 = -\frac{1}{2}\gamma \nabla (\mathbf{u}_0 \cdot \mathbf{u}_0) \\ \rho_1 = p_1/\gamma \\ \dfrac{\partial^2 \psi_1}{\partial r^2} - \dfrac{1}{r}\dfrac{\partial \psi_1}{\partial r} + \dfrac{\partial^2 \psi_1}{\partial z^2} = -\rho_1 \dfrac{\partial^2 \psi_0}{\partial r^2} + \dfrac{1}{r}\rho_1 \dfrac{\partial \psi_0}{\partial r} - \rho_1 \dfrac{\partial^2 \psi_0}{\partial z^2} + \dfrac{\partial \rho_1}{\partial r}\dfrac{\partial \psi_0}{\partial r} + \dfrac{\partial \rho_1}{\partial z}\dfrac{\partial \psi_0}{\partial z} \end{cases}. \tag{60}$$

Clearly, the first compressible correction for the pressure field may be directly integrated from Euler's first-order equation to return

$$p_1 = -\tfrac{1}{2}\gamma(r^2 + 4z^2). \tag{61}$$

Next, the density may be extracted from the isentropic relation,

$$\rho_1 = p_1/\gamma = -\tfrac{1}{2}(r^2 + 4z^2). \tag{62}$$

At this point, backward substitution into Eq. (60) unravels the first-order representation of the vorticity equation,

$$\frac{\partial^2 \psi_1}{\partial r^2} - \frac{1}{r}\frac{\partial \psi_1}{\partial r} + \frac{\partial^2 \psi_1}{\partial z^2} = -6r^2 z. \tag{63}$$

We also find it useful to express the first-order velocity in terms of the streamfunction. The corresponding terms proceed from the perturbed form of Eq. (55), specifically

$$u_r^{(1)} = -\rho_1 u_r^{(0)} - \frac{1}{r}\frac{\partial \psi_1}{\partial z} \quad \text{and} \quad u_z^{(1)} = -\rho_1 u_z^{(0)} + \frac{1}{r}\frac{\partial \psi_1}{\partial r}. \tag{64}$$

As for the boundary conditions, they conveniently translate into

$$\begin{cases} \psi_1(0,0)=0 \\ u_r^{(1)}(0,z)=0, \quad \lim\limits_{r\to 0}\dfrac{1}{r}\dfrac{\partial\psi_1(0,z)}{z}=0 \\ u_r^{(1)}(1,z)=0, \quad \dfrac{\partial\psi_1(1,z)}{\partial z}=-\frac{1}{2}-2z^2 \\ u_z^{(1)}(r,0)=0, \quad \dfrac{1}{r}\dfrac{\partial\psi_1(r,0)}{r}=0 \end{cases}. \tag{65}$$

The solution for ψ_1 may be constructed from a linear combination of additive and multiplicative separation of variables. Using the boundary conditions and the right-hand side of Eq. (63) as a guide, it is expedient to start with

$$\psi_1(r,z)=a_0+a_1r^2z+a_2r^4z+a_3r^2z^3, \tag{66}$$

where the coefficients may be systematically obtained from Eq. (65). At length, we arrive at

$$\psi_1(r,z)=-\tfrac{1}{4}r^2z-\tfrac{1}{4}r^4z-\tfrac{2}{3}r^2z^3 \tag{67}$$

with the first-order velocity being

$$\begin{cases} u_r^{(1)}=\frac{1}{4}r(1-r^2) \\ u_z^{(1)}=\frac{1}{6}z(16z^2-3) \end{cases}. \tag{68}$$

It is gratifying that Eq. (68) proves to be equivalent to the solution obtained using the potential formulation in Eq. (47).

At this juncture, the second-order pressure may be determined as well. It may be extracted from the second-order Euler equation,

$$\nabla p_2=-\tfrac{1}{2}\gamma\rho_1\nabla(\mathbf{u}_0\cdot\mathbf{u}_0)-\gamma\nabla(\mathbf{u}_0\cdot\mathbf{u}_1), \tag{69}$$

thus yielding

$$p_2=-\gamma\left[\tfrac{1}{8}\left(r^4-2r^2\right)-r^2z^2+\tfrac{10}{3}z^4-z^2\right]. \tag{70}$$

This result concurs with Eq. (51) in the velocity potential formulation.

V. COMPRESSIBLE SUCTION DOMINATED SELLARS MOTION

The reverse flow problem associated with compressible motion in a porous cylinder with large wall suction can be treated using either of the two methodologies presented above. The incompressible profile arising in such a configuration stems from Berman's similarity transformation and depends on the suction Reynolds number. In our case, this may be written as $Re=\rho U_w a/\mu$, where $U_w<0$ for suction. While Berman managed to develop approximations for small Reynolds numbers,[2] his work was extended by Yuan[22,52] in both planar and axisymmetric geometries to $Re\approx 20$, while Sellars,[53] and Terrill and Thomas[54] produced exact solutions as the Reynolds number became large. The exact profile by Sellars,[53] namely $\phi=\frac{1}{2}r^2-z^2$, is of particular interest because it emerges at $Re\to\infty$ and may be promptly recovered from the Hart-McClure model by modifying the sidewall boundary condition to reflect the opposite direction. The ensuing streamlines are illustrated in Fig. 2 along with Hart-McClure's. To obtain the compressible Sellars mean flow, the radial boundary condition must be modified to

$$u_r(1,z)=\frac{\partial\phi(1,z)}{\partial r}=-\frac{1}{\rho r}\frac{\partial\psi(1,z)}{\partial z}=1. \tag{71}$$

However, the potential and streamfunction equations themselves need not be altered.

The general leading-order solution given by Eq. (26) translates identically for the suction-driven flowfield. The only boundary condition that changes occurs at the sidewall, thus leading to $C_1=C_2$

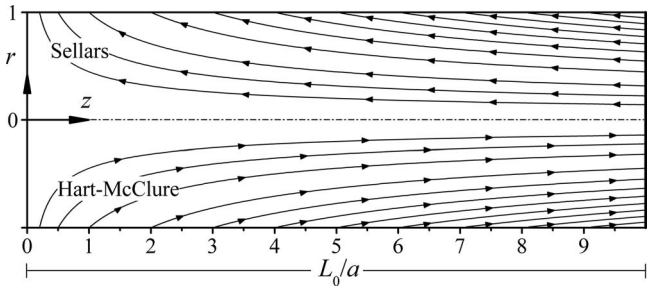

FIG. 2. Streamlines for the suction-based Sellars profile versus the injection-based Hart-McClure mean flow.

$= C_3 = C_4 = 0$. Applying Eq. (71) provides the last remaining constant, $\upsilon = 2$. The final form of the leading-order potential function collapses into

$$\phi_0 = \tfrac{1}{2}r^2 - z^2. \tag{72}$$

Equation (72) represents the incompressible Sellars profile.[53] The compressible correction follows a similar procedure, though the first-order potential equation varies due to the leading-order contribution,

$$\frac{\partial^2\phi_1}{\partial r^2} + \frac{1}{r}\frac{\partial\phi_1}{\partial r} + \frac{\partial^2\phi_1}{\partial z^2} = r^2 - 8z^2. \tag{73}$$

As before, Eq. (73) can be readily solved by separation of variables such that a general expression for ϕ_1 may be returned,

$$\phi_1 = \kappa\frac{r^2}{4} + \frac{r^4}{16} + K_1 \ln r + K_2 - \frac{2}{3}z^4 - \frac{\kappa}{2}z^2 + K_3 z + K_4. \tag{74}$$

The boundary conditions for the compressible correction remain identical to the injection flow analogue. Evaluating Eq. (74) using the auxiliary conditions given by Eq. (43) yields

$$\phi_1 = -\frac{r^2}{8} + \frac{r^4}{16} - \frac{2}{3}z^4 + \frac{1}{4}z^2. \tag{75}$$

The compressible correction for the Sellars mean flow is therefore identical but opposite in sign to that of Hart-McClure. The same outcome may be realized using the vorticity-streamfunction approach. In what follows, the focus will be shifted back to the injection dominated model.

VI. RESULTS AND DISCUSSION

A. Potential lines

Figure 3 shows the potential lines for a reference case of $M_w = 0.01$. In Fig. 3(a) the effects of compressibility are presented as a leftward shift of the potential lines. Little change in curvature may be seen to accompany the potential lines as the flow in the downstream region is predominantly axial. Figure 3(b) presents a more detailed view of the potential lines near the head end of the chamber. Here, the axial and radial velocities are of the same order, resulting in increased curvature of the potential lines. The diagonal crossing the origin demarcates the border between radial and axial dominance of the flow. As expected, the compressibility effects in this region are virtually nonexistent as the compressible and incompressible potential lines nearly coincide.

B. Critical length and universal similarity

Characterizing the critical length, also called the sonic length, is an integral measure to compare the present study to existing experimental and computational data. By normalizing the length of a motor by the critical length, it is possible to compare the analytical predictions directly to numerical or experimental data, provided that the choking length is known. Past solutions have also displayed

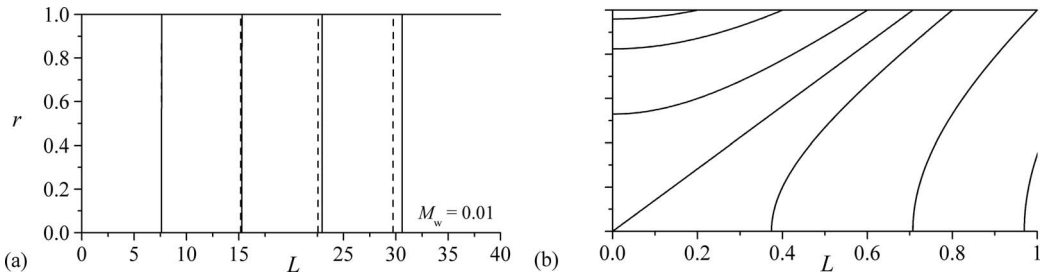

FIG. 3. Potential lines for the compressible (dashed) and incompressible solutions (solid) depicting the spatial evolution of the solution in (a) a long chamber and (b) the headwall region; here $M_w = 0.01$.

similarity behavior when normalized by the critical length in so far as the wall Mach number remains small. This similarity is especially useful when weighing multiple models against one another as only a single Mach number is necessary for a complete comparison. With these notions in mind, we examine the dimensional quantities leading to

$$\frac{\bar{u}_z}{c} = 1. \tag{76}$$

Equation (76) provides the criterion for the critical length. When the dimensional axial velocity divided by the local speed of sound reaches unity, the choking condition is satisfied. Rewriting Eq. (76) in terms of our dimensionless solution and squaring both sides, we have

$$\frac{u_z^2}{T}\frac{U_w^2}{\gamma R T_0} = 1. \tag{77}$$

The reference constants may be collected to retrieve

$$M_w^2 u_z^2 = T. \tag{78}$$

At this juncture, we may insert the Rayleigh-Janzen expansion into Eq. (78) to obtain

$$M_w^2\left(\frac{\partial\phi_0}{\partial z}\right)^2 + M_w^4\frac{\partial\phi_0}{\partial z}\frac{\partial\phi_1}{\partial z} + M_w^6\left(\frac{\partial\phi_1}{\partial z}\right)^2 = 1 + M_w^2 T_1 + M_w^4 T_2. \tag{79}$$

Next, we may expand Eq. (79) with the known quantities for the potential function and temperature while ignoring the slight radial dependence; we find

$$4z^2M_w^2 + 4z(\tfrac{8}{3}z^3 - \tfrac{1}{2}z)M_w^4 + \left(\tfrac{8}{3}z^3 - \tfrac{1}{2}z\right)^2 M_w^6 = 1 - 2(\gamma-1)z^2M_w^2 - \tfrac{1}{3}(\gamma-1)z^2\left(16z^2-3\right)M_w^4. \tag{80}$$

Equation (80) represents a cubic polynomial in z that leads to a tedious expression. An asymptotically equivalent solution (in which higher-order Mach number corrections are dismissed) may be extracted in lieu of the full expression, namely,

$$L_s = \sqrt{\frac{1}{8} - \frac{\gamma+1}{4M_w^2} + \frac{8(2\gamma^2+\gamma-1) - 4(\gamma+1)M_w^2 + M_w^4 + 2^{2/3}4\alpha^2}{32M_w^2 2^{1/3}\alpha}}, \tag{81}$$

where L_s stands for the critical sonic length and α denotes a constant based purely on the ratio of specific heats,

$$\alpha = [23 + 6\gamma - 3\gamma^2 - 4\gamma^3 + 3(59 + 30\gamma - 12\gamma^2 - 22\gamma^3 - 3\gamma^4)^{\frac{1}{2}}]^{1/3}. \tag{82}$$

The difference between Eq. (81) and the full solution is limited to a single digit variance in the fourth decimal place.

This result is compared in Fig. 4 to the compressible study by Majdalani[1] where a similar sonic length calculation is deduced. For all cases, the present work requires a longer chamber to reach choked flow conditions. If a mass balance is conducted between the two models, for a given sinusoidal profile, the equivalent plug flow velocity will be lower than the maximum velocity of the

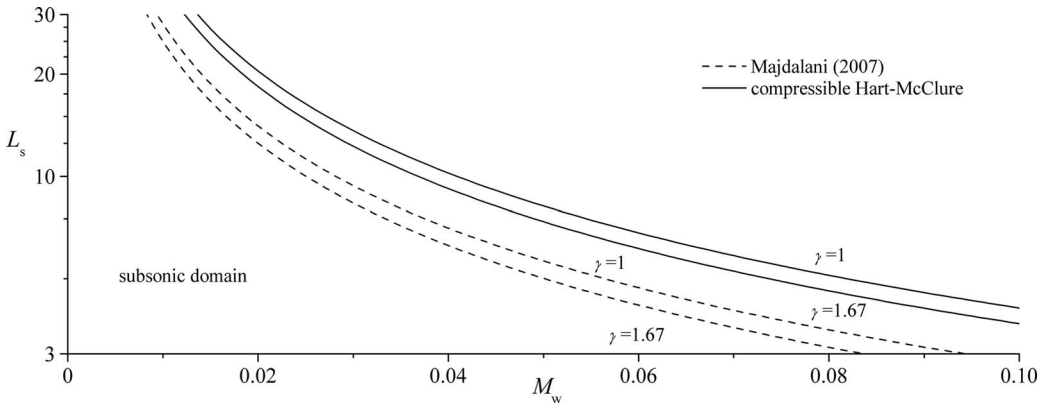

FIG. 4. Critical length over a range of injection Mach numbers.

rotational counterpart. It is therefore expected that a higher centerline velocity will reach choked conditions sooner than the slower irrotational analogue. This behavior is consistent across the range of specific heat ratios. The sonic length is again found to be weakly dependent on the specific heats ratio, with larger values of γ leading to shorter L_s.

C. Comparison to other compressible models

In recent work, Majdalani[1] assumes uniform sidewall injection in a right-cylindrical chamber to obtain the compressible, axisymmetric analogue of Taylor-Culick's profile. In the interest of clarity, the main ingredients of his solution are reproduced below:

$$\psi = M_w \psi_0 \left(1 - \tfrac{1}{4}\Gamma^2\left[1 + \tfrac{1}{3}\cos(\pi r^2)\right]\chi^2 + \tfrac{1}{2}M_w^2\right), \quad \psi_0 \equiv z\sin(\tfrac{1}{2}\pi r^2),$$
$$\chi \equiv z/L_s \text{ (streamfuntion)}, \tag{83}$$

$$M_c = \Gamma\chi\frac{2 + \tfrac{1}{3}\Gamma^2\chi^2 - M_w^2}{\sqrt{4 - 2(\gamma-1)\Gamma^2\chi^2}}, \text{ (centerline Mach number)}, \tag{84}$$

$$p_c = 1 - \tfrac{1}{2}\gamma\,\Gamma^2\chi^2(1 - M_w^2) - \tfrac{1}{24}\gamma\,\Gamma^4\chi^4 \text{ (centerline pressure)}, \tag{85}$$

$$T_c = 1 - \tfrac{1}{2}(\gamma-1)\Gamma^2\chi^2(1 - M_w^2) - \tfrac{1}{6}(\gamma-1)\Gamma^4\chi^4 \text{ (centerline temperature)}, \tag{86}$$

where the sonic length, also known as the critical distance, is related to the Γ function through

$$\Gamma \equiv \pi M_w L_s = \sqrt{\lambda - 2\gamma - 2 + 2(2\gamma^2 + \gamma - 1)/\lambda}$$
$$\cong 0.884622 - 0.177299(\gamma-1) + 0.0539119(\gamma-1)^2 - 0.0180615(\gamma-1)^3, \tag{87}$$

and

$$\lambda = \left(28 + 12\gamma - 6\gamma^2 - 8\gamma^3 + 6\sqrt{22 + 18\gamma - 6\gamma^2 - 14\gamma^3 - 3\gamma^4}\right)^{1/3}. \tag{88}$$

By retaining the leading-order term, we can also compare the solution to the incompressible Taylor-Culick flow.

A comparison to the one-dimensional model used by Gany and Aharon[18] is also beneficial. Owing to the irrotational nature of the present study, the velocity components remains one-dimensional, even though the model itself is axisymmetric. Gany and Aharon[18] focus their analysis on the chamber pressure, which they express as

$$p = \frac{1 + \gamma\left[1 - (z/L_s)^2\right]^{1/2}}{\gamma + 1}. \tag{89}$$

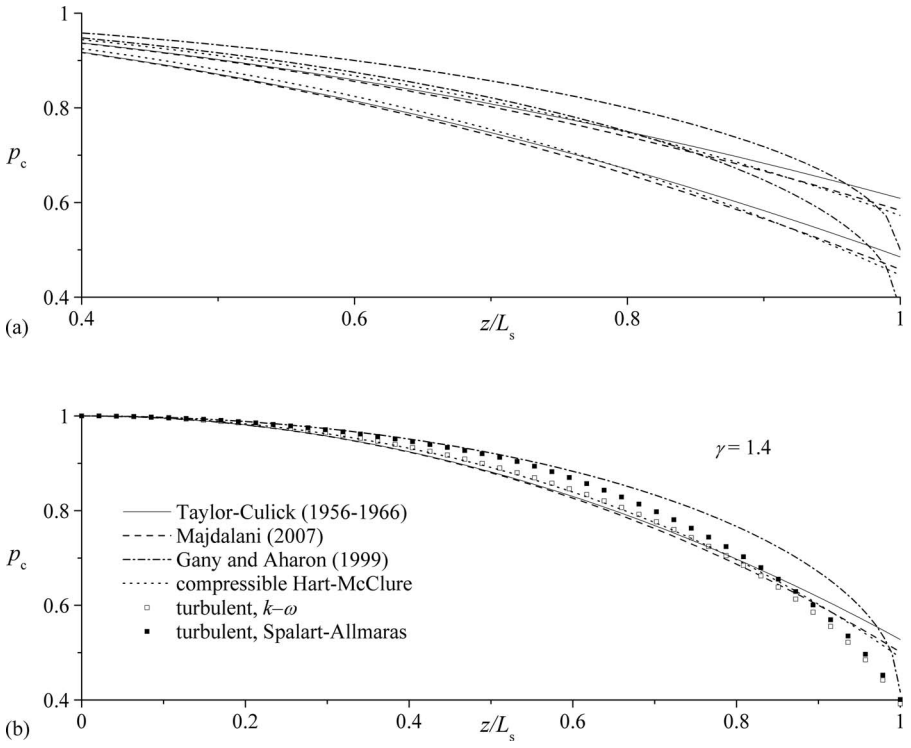

FIG. 5. Centerline pressure profiles given (a) variations in γ that start for each curve with $\gamma = 1$ (top) and 1.67 (bottom), and (b) fixed $\gamma = 1.4$ with additional CFD data (square symbols). Otherwise, both parts share the same legend.

Figure 5(a) highlights the centerline pressure over a range of specific heats ratios. The present model displays a similar shape to the existing models that observe the established γ dependence. Near the exit plane of the chamber, the compressible solution exhibits a steeper curvature that strikingly mimics the slope of the one-dimensional model. This behavior may be expected as the streamwise velocity dominates towards the aft end of the chamber, hence providing an approximation that approaches that of one-dimensional axial motion. In Fig. 5(b), a single specific heats ratio, $\gamma = 1.4$, is featured along with the addition of two CFD solutions calculated using a finite volume Navier-Stokes solver. The concurrence of the present solution with the $k - \omega$ model is particularly satisfying. That such a reduced formulation can capture these pressure effects so well lends support to the viability of using simplified mean flow models in SRM analysis.

Figure 6 illustrates the spatial distribution of the axial velocities compared to the rotational Taylor-Culick and its compressible counterpart. The velocities are displayed at ten percent increments of the sonic length and renormalized by their maximum velocity. The compressible results coincide at the critical point and agree well in the second half of the chamber, as the present and previous compressible studies have nearly identical values along the centerline. Figure 6 also confirms a

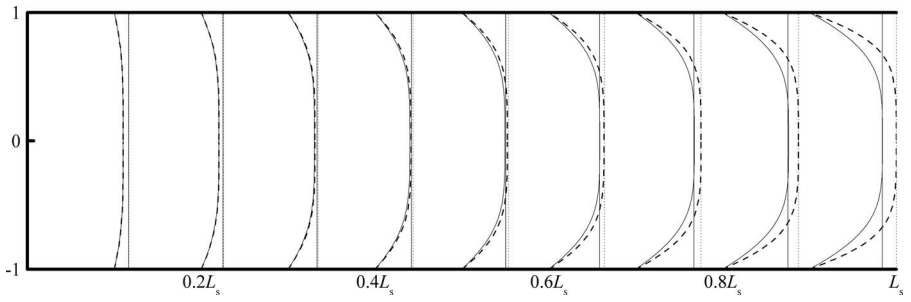

FIG. 6. Axial velocity evolution of the Hart-McClure (dotted), the Taylor-Culick (solid), and the compressible Taylor-Culick models (dashed).

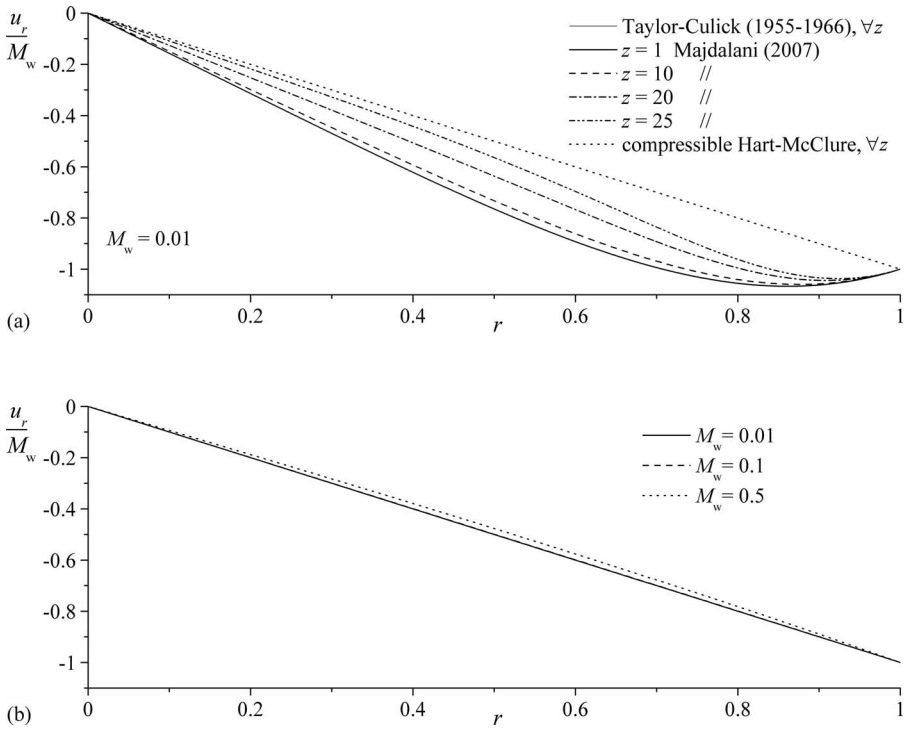

FIG. 7. Radial velocity of the Hart-McClure model (a) compared to the compressible Taylor-Culick mean flow and (b) shown over a range of injection Mach numbers.

previous finding: the onset of compressibility occurs near the midpoint of the chamber. Near the fore end of the chamber, the relative magnitudes slightly disagree with the Hart-McClure prediction, showing larger velocities at the same fraction of the sonic length. The incompressible velocity displays similar trends, thereby implying that the discrepancy is not a result of compressibility, but rather the difference in velocity development between rotational and irrotational flowfields.

Unlike the rotational approximation of the compressible Taylor-Culick motion,[1] the radial velocity here appears as a sole function of r, thus obviating the need for axial case comparisons. Figure 7(a) sets our solution against the radial velocity identified by Majdalani[1] using $M_w = 0.01$. The present u_r may be seen to be practically linear and quite insensitive to the wall Mach number. The corresponding curve acts as an "upper" bound on the radial velocity solutions. Clearly, as the compressible Taylor-Culick profile develops in the streamwise direction, it slowly approaches the irrotational model. Figure 7(b) highlights the effects of compressibility on the radial velocity. Accordingly, one infers that for a practical range of injection Mach numbers, the incompressible solution may be sufficient to describe the radial flow behavior. When the injection Mach number is raised, the radial velocity responds with an increase in the quarter-radius region. Nevertheless, the increase is so slight that it may be safely ignored, especially when compared to the more dominant axial velocity.

To complete the velocity analysis, the Mach number distribution in the chamber may be determined from a judicious expansion of Eq. (78). Rather than equating the left-hand side of Eq. (78) to unity in the calculation of the sonic length, a more general $M(r, z)$ may be retained on the right-hand side. By solving the ensuing equation, an expression for the local Mach number may be obtained, specifically

$$M(r,z) = \frac{M_w z\left[\left(\frac{16}{3}z^2 - 1\right)M_w^2 + 4\right]}{\sqrt{4 - (\gamma-1)M_w^2\left\{\left(2 - M_w^2 + M_w^2 r^2\right)r^2 + 4z^2\left[2 + \left(\frac{16}{3}z^2 - 1\right)M_w^2\right]\right\}}} \tag{90}$$

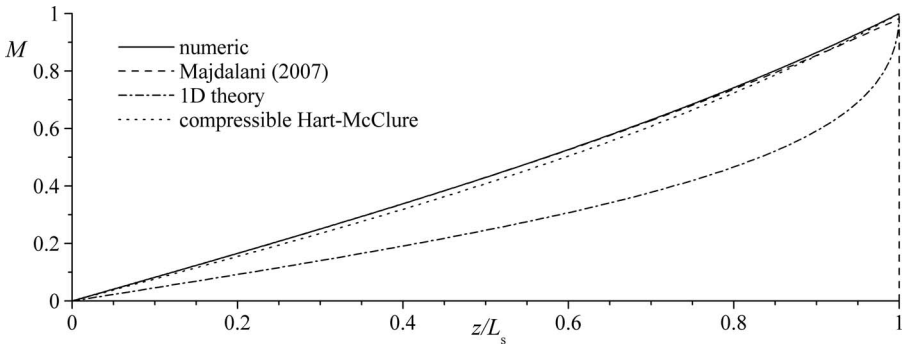

FIG. 8. Mach number distribution over the chamber length.

and so, at the centerline,

$$M_c(z) = \frac{M_w z\left[4 + \left(\frac{16}{3}z^2 - 1\right)M_w^2\right]}{2\sqrt{1 - (\gamma - 1)M_w^2 z^2\left[2 + \left(\frac{16}{3}z^2 - 1\right)M_w^2\right]}}. \tag{91}$$

Figure 8 shows that the Mach number distributions match admirably. The only outlier corresponds to the one-dimensional model for which a uniformly lower Mach number is predicted everywhere except in the proximity of the sonic point. With the present study agreeing more closely with the rotational solutions, the difference in Mach number distributions may be attributed to the one-dimensionality of the solution, rather than its irrotationality. It is hence preferred over the strictly 1D model in which no radial variations occur. As for the ability to incorporate variable headwall injection, the compressible Hart-McClure approximation offers the flexibility to absorb an arbitrary injection pattern that may be specified at $z = 0$. The possibility of introducing a rotational injection profile at entry may be justified by the approximate nature of the compressible mean flow obtained asymptotically and the ramifications of using an arbitrary injection pattern on the accuracy of the resulting formulation. Additional detail regarding the error associated with the use of a rotational profile at entry may be found in work by Majdalani and Saad,[23] Kurdyumov,[24] and Saad and Majdalani.[55]

VII. CONCLUSIONS

In this study, the compressible extension to the Hart-McClure model is developed, employing a Rayleigh-Janzen expansion in the injection Mach number squared. The resulting equations are solved analytically to produce an asymptotic solution that properly captures the effects of compressibility. In the process, both potential and vorticity-streamfunction formulations of the problem are pursued and shown to yield equivalent results. These frameworks are carefully developed from first principles and then solved using different mathematical approaches that depend on either additive or multiplicative forms of the separation of variables technique. This study is thus unique in its presentation of two alternative approaches that can be used to obtain compressible flow corrections to a variety of potential motions. After confirming the accuracy of the resulting approximation, our solution is compared to other compressible flow studies, including the one-dimensional Gany and Aharon model[18] as well as the axisymmetric, compressible Taylor-Culick analogue provided by Majdalani.[1] The compressible form of the suction-driven Sellars profile is also discussed in passing.

The compressible models exhibit agreement over a range of operating conditions. The pressure and Mach number evaluations, in particular, are satisfying in their correspondence. By comparing the compressible rotational and irrotational models, the multifaceted effects that compressibility bears on these different profiles are clarified. The most notable contrasts occur between the velocity fields. The radial component of the compressible Hart-McClure velocity can be approximated as incompressible with no ill effects, whereas the same profile in the rotational case undergoes appreciable alterations in shape during the compressible steepening process. The amplification levels of the axial velocities in both compressible studies remain consistent with each other, although the

Hart-McClure motion displays a slight shift near the headwall that may be attributed to its irrotational character.

The asymptotic predictions presented here consist of basic compressibility corrections. Evaluation of higher-order terms may provide a better understanding of the suitability of Rayleigh-Janzen expansions as the mean flow Mach number increases. Unlike the rotational equations whose complexity can prevent such an effort, the irrotational approximations can be extended to higher orders with relative ease, though such an extension falls beyond the scope of this work. Furthermore, an extension of both compressible models to account for alternate geometries and time-dependent features, such as wall regression, may be interesting prospects for future work.

ACKNOWLEDGMENTS

This work was sponsored by the National Science Foundation and the H. H. Arnold Chair of Excellence in Advanced Propulsion, the University of Tennessee Space Institute.

[1] J. Majdalani, "On steady rotational high speed flows: The compressible Taylor-Culick profile," Proc. R. Soc. London, Ser. A **463**, 131–162 (2007).
[2] M. Hill, "On a spherical vortex," Phil. Trans. R. Soc. London, Ser. A **185**, 213–245 (1894).
[3] D. Moore and D. Pullin, "On steady compressible flows with compact vorticity; the compressible Hill's spherical vortex," J. Fluid Mech. **374**, 285–303 (1998).
[4] B. A. Maicke and J. Majdalani, "On the rotational compressible Taylor flow in injection-driven porous chambers," J. Fluid Mech. **603**, 391–411 (2008).
[5] T. Saad and J. Majdalani, "On the Lagrangian optimization of wall-injected flows: From the Hart–McClure potential to the Taylor–Culick rotational motion," Proc. R. Soc. London, Ser. A **466**, 331–362 (2010).
[6] T. Saad and J. Majdalani, "Extension of Kelvin's minimum energy theorem to flows with open regions," AIAA Paper 2010-4287, 2010.
[7] B. Wasistho, S. Balachandar, and R. Moser, "Compressible wall-injection flows in laminar, transitional, and turbulent regimes: Numerical prediction," J. Spacecr. Rockets **41**, 915–924 (2004).
[8] J. Majdalani and W. Van Moorhem, "Improved time-dependent flowfield solution for solid rocket motors," AIAA J. **36**, 241–248 (1998).
[9] F. Chedevergne, G. Casalis, and J. Majdalani, "Direct numerical simulation and biglobal stability investigations of the gaseous motion in solid rocket motors," J. Fluid Mech. **706**, 190–218 (2012).
[10] P. Venugopal, R. Moser, and F. Najjar, "Direct numerical simulation of turbulence in injection-driven plane channel flows," Phys. Fluids **20**, 105103 (2008).
[11] R. A. Beddini, "Injection-induced flows in porous-walled ducts," AIAA J. **24**, 1766–1773 (1986).
[12] J. Sabnis, H. Gibeling, and H. McDonald, "Navier-Stokes analysis of solid propellant rocket motor internal flows," J. Propul. Power **5**, 657–664 (1989).
[13] T. Liou and W. Lien, "Numerical simulations of injection-driven flows in a two-dimensional nozzleless solid-rocket motor," J. Propul. Power **11**, 600–606 (1995).
[14] J. C. Traineau, P. Hervat, and P. Kuentzmann, "Cold-flow simulation of a two-dimensional nozzleless solid-rocket motor," AIAA Paper No. 86-1447, 1986.
[15] G. Balakrishnan, A. Liñan, and F. A. Williams, "Rotational inviscid flow in laterally burning solid propellant rocket motors," J. Propul. Power **8**, 1167–1176 (1992).
[16] G. Balakrishnan, A. Liñan, and F. A. Williams, "Compressible effects in thin channels with injection," AIAA J. **29**, 2149–2154 (1991).
[17] M. Akiki and J. Majdalani, "Improved integral form of the compressible flowfield in thin channels with injection," AIAA J. **50**, 485–493 (2012).
[18] A. Gany and I. Aharon, "Internal ballistics considerations of nozzleless rocket motors," J. Propul. Power **15**, 866–873 (1999).
[19] F. McClure, R. Hart, and R. Cantrell, "Interaction between sound and flow: Stability of T-burners," AIAA J. **1**, 586–590 (1963).
[20] G. Taylor, "Fluid flow in regions bounded by porous surfaces," Proc. R. Soc. London, Ser. A **234**, 456–475 (1956).
[21] F. Culick, "Rotational axisymmetric mean flow and damping of acoustic waves in a solid propellant rocket," AIAA J. **4**, 1462–1464 (1966).
[22] S. Yuan and A. Finkelstein, "Laminar pipe flow with injection and suction through a porous wall," Trans. ASME: J. Appl. Mech. **78**, 719–724 (1956).
[23] J. Majdalani and T. Saad, "The Taylor-Culick profile with arbitrary headwall injection," Phys. Fluids **19**, 093601 (2007).
[24] V. N. Kurdyumov, "Viscous and inviscid flows generated by wall-normal injection into a cylindrical cavity with a headwall," Phys. Fluids **20**, 123602 (2008).
[25] O. C. Sams, J. Majdalani, and T. Saad, "Mean flow approximations for solid rocket motors with tapered walls," J. Propul. Power **23**, 445–456 (2007).
[26] V. Kurdyumov, "Steady flows in the slender, noncircular, combustion chambers of solid propellants rockets," AIAA J. **44**, 2979–2986 (2006).
[27] J. Majdalani, A. Vyas, and G. Flandro, "Higher mean-flow approximation for a solid rocket motor with radially regressing walls," AIAA J. **40**, 1780–1788 (2002).

[28] J. Majdalani, A. Vyas, and G. Flandro, "Erratum on higher mean-flow approximation for a solid rocket motor with radially regressing walls," AIAA J. **47**, 286–286 (2009).
[29] C. Zhou and J. Majdalani, "Improved mean-flow solution for slab rocket motors with regressing walls," J. Propul. Power **18**, 703–711 (2002).
[30] H. Xu, Z. Lin, S. Liao, J. Wu, and J. Majdalani, "Homotopy based solutions of the Navier-Stokes equations for a porous channel with orthogonally moving walls," Phys. Fluids **22**, 053601 (2010).
[31] C. Berbente, S. Dănăilă, and S. Berbente, "Analytic solutions for axisymmetric incompressible flows with wall injection and regression," P. Romanian Acad. A **12**, 221–229 (2011).
[32] R. Hart and F. McClure, "Combustion instability: Acoustic interaction with a burning propellant surface," J. Chemical Phys. **30**, 1501–1514 (1959).
[33] R. Hart and F. McClure, "Theory of acoustic instability in solid propellant rocket combustion," Int. Symp. Combust. **10**, 1047–1066 (1965).
[34] F. McClure, R. Hart, and J. Bird, "Acoustic resonance in solid propellant rockets," J. Appl. Phys. **31**, 884–896 (1960).
[35] R. H. Cantrell, R. W. Hart, and F. T. McClure, "Acoustic energy losses in rocket-engine cavities," J. Acoust. Soc. Am. **35**, 773–773 (1963).
[36] R. Hart and R. Cantrell, "Amplification and attenuation of sound by burning propellants," AIAA J. **1**, 398–404 (1963).
[37] R. H. Cantrell and R. W. Hart, "Interaction between sound and flow in acoustic cavities: Mass, momentum, and energy considerations," J. Acoust. Soc. Am. **36**, 697–706 (1964).
[38] R. Hart, J. Bird, R. Cantrell, and F. McClure, "Nonlinear effects in instability of solid-propellant rocket motors," AIAA J. **2**, 1270–1273 (1964).
[39] G. Flandro and J. Majdalani, "Aeroacoustic instability in rockets," AIAA J. **41**, 485–497 (2003).
[40] S. Fischbach, J. Majdalani, and G. Flandro, "Acoustic instability of the slab rocket motor," J. Propul. Power **23**, 146–157 (2007).
[41] J. Majdalani, G. A. Flandro, and S. R. Fischbach, "Some rotational corrections to the acoustic energy equation in injection-driven enclosures," Phys. Fluids **17**, 074102 (2005).
[42] J. Majdalani, S. Fischbach, and G. Flandro, "Improved energy normalization function in rocket motor stability calculations," Aerosp. Sci. Technol. **10**, 495–500 (2006).
[43] G. Flandro, S. Fischbach, and J. Majdalani, "Nonlinear rocket motor stability prediction: Limit amplitude, triggering, and mean pressure shift," Phys. Fluids **19**, 094101 (2007).
[44] J. Majdalani and M. Akiki, "Rotational and quasiviscous cold flow models for axisymmetric hybrid propellant chambers," ASME J. Fluids Eng. **132**, 101202 (2010).
[45] J. Majdalani, "Analytical Models for Hybrid Rockets," in *Fundamentals of Hybrid Rocket Combustion and Propulsion*, edited by K. Kuo and M J Chiaverini (AIAA Progress in Astronautics and Aeronautics, Washington, DC, 2007), pp. 207–246.
[46] W. A. Khan, J. R. Culham, and M. M. Yovanovich, "Analytical study of heat transfer from circular cylinder in liquid metals," Heat Mass Trans. **42**, 1017–1023 (2006).
[47] J. Majdalani, "Reply to Robert L. Glick's comment: Physicality of core flow models in rocket motors," J. Propul. Power **19**, 156–159 (2003).
[48] J. Majdalani, G. Flandro, and T. Roh, "Convergence of two flowfield models predicting a destabilizing agent in rocket combustion," J. Propul. Power **16**, 492–497 (2000).
[49] R. L. Bayt, A. A. Ayon, and K. S. Breuer, "A performance evaluation of MEMS-based micronozzles," AIAA Paper No. 97-3169, 1997.
[50] L. Ren, D. Sinton, and D. Li, "Numerical simulation of microfluidic injection processes in crossing microchannels," J. Micromech. Microeng. **13**, 739–747 (2003).
[51] A. H. Shapiro, *The Dynamics and Thermodynamics of Compressible Fluid Flow* (Ronald, 1953).
[52] S. Yuan, "Further investigation of laminar flow in channels with porous walls," J. Appl. Phys. **27**, 267–269 (1956).
[53] J. Sellars, "Laminar flow in channels with porous walls at high suction Reynolds numbers," J. Appl. Phys. **26**, 489–490 (1955).
[54] R. Terrill and P. Thomas, "On laminar flow through a uniformly porous pipe," Appl. Sci. Res. **21**, 37–67 (1969).
[55] T. Saad and J. Majdalani, "Rotational flowfields in porous channels with arbitrary headwall injection," J. Propul. Power **25**, 921–929 (2009).